Forschungszentrum Karlsruhe
in der Helmholtz-Gemeinschaft

Wissenschaftliche Berichte
FZKA 7054

Complementary Experiments at the Karlsruhe Dynamo Test Facility

U. Müller, R. Stieglitz, S. Horanyi
Institut für Kern- und Energietechnik

November 2004

Forschungszentrum Karlsruhe

in der Helmholtz-Gemeinschaft

Wissenschaftliche Berichte

FZKA 7054

Complementary experiments at the Karlsruhe dynamo test facility

U. Müller*, R. Stieglitz, S. Horanyi**

Institut für Kern- und Energietechnik

*Universität Karlsruhe

**Atomic Energy Research Institute, Budapest

Forschungszentrum Karlsruhe GmbH, Karlsruhe

2004

Impressum der Print-Ausgabe:

Als Manuskript gedruckt

Forschungszentrum Karlsruhe GmbH
Postfach 3640, 76021 Karlsruhe

Mitglied der Hermann von Helmholtz-Gemeinschaft
Deutscher Forschungszentren (HGF)

ISSN 0947-8620

urn:nbn:de:0005-070543

Complementary experiments at the Karlsruhe dynamo test facility

Abstract

The article reports experimental results on dynamo action obtained at the Karlsruhe dynamo test facility. Former observations concerning the properties of the dynamo magnetic field are corroborated and complemented. The feedback of the dynamo magnetic field on the sodium velocity in the test module is analysed based on measurements employing permanent magnet potential sensors. The evaluation of time signals recorded by these probes shows that a growing dynamo magnetic field transforms hydrodynamic turbulent velocity profiles in channels into magnetohydrodynamic slug flow profiles, indicating a balance between pressure and Lorentz forces mainly. Cross-correlations between time signals of the magnetic induction and the local velocity reveal a significant coherency between apparently random fluctuations of these relevant dynamo quantities.

Ergänzende Experimente am Karlsruher Dynamo-Versuchsstand

Zusammenfassung

In diesem Bericht werden weitere experimentelle Ergebnisse von der Karlsruher Dynamo-Versuchseinrichtung vorgestellt. Frühere Beobachtungen über Eigenschaften des Dynamo-Magnetfeldes werden bestätigt und ergänzt. Die Rückkopplung des magnetischen Feldes auf die Natriumströmung in der Versuchsapparatur wird durch Messungen mit Permanentmagnet-Potentialsonden analysiert. Die Auswertung der Signale dieser Sonden zeigt, dass ein wachsendes Dynamo-Magnetfeld ein turbulentes Geschwindigkeitsprofil in eine magnetohydrodynamische Kolbenströmung überführt. Dies ist im wesentlichen auf ein Gleichgewicht zwischen Druck- und Lorentz-Kräften zurückzuführen. Kreuzkorrelationen zwischen Zeitsignalen der Magnetfeldstärke und der Geschwindigkeit geben Hinweise auf eine signifikante Kohärenz zwischen diesen Grössen.

Contents

1. Introduction

It is generally accepted today that planetary and stellar magnetic fields originate from dynamo action in homogeneous, electrically conducting and circulating fluids in the interior of celestial bodies. This idea was first conjectured by Lamor (1919) and has been corroborated repeatedly by several geo- and astrophysicists who developed analytical and numerical models for this magnetohydrodynamic process. Spectacular numerical calculations simulate even sophisticated geo- and astrophysical phenomena such as reversals of the geomagnetic field and the magnetodynamics of solar flairs. The progress in the development of dynamo modelling has been repeatedly summarized in survey articles, e.g. by Rädler (1999), Busse (2000), Glatzmaier and Roberts (2001) and in a recent textbook by Rüdiger & Hollerbach (2004). There has always been the desire to confirm the models for homogeneous dynamo action in laboratory experiments. For principle reasons such experiments require dimensions of equipment that commonly exceed the capability of University Laboratories and may even challenge the technologies of major research establishments. Stieglitz & Müller (1996) as well as Cardin et al. (2002) have outlined this in some detail.

Loves & Wilkinson (1968) first demonstrated experimentally the feasibility of homogeneous dynamos in electrically conducting continua. They avoided the problem of big devices by using ferromagnetic material and employing rigid body rotation of solid steel cylinders in steel blocks (lubricated by liquid mercury at contacting boundaries). They followed a model conception of Herzberg (1958) to achieve self-excitation of dynamo action. The design of an experimental hydromagnetic screw dynamo was pursued by Gailitis et al. (1989) in Riga taking up an idea of Ponomarenko (1973). They showed successfully (Gailitis et al. 2000, 2001) that dynamo magnetic fields could be generated by helical sodium flow in a coaxial pipe. A next step towards

more generic flow topologies regarding geophysical application was done in the Karlsruhe dynamo experiment (Stieglitz, Müller 2001, Müller, Stieglitz, Horanyi 2004). Here, according to a proposal by Busse (1992), an arrangement of counter rotating columnar vortices was realized by forced flow in a system of helical guide tubes placed in a container filled with sodium. In several test campaigns a permanent dynamo magnetic field of dipole character was observed at this test facility and was analysed in some detail (Müller et al. 2004). The successful dynamo experiments in Riga and Karlsruhe have stimulated efforts of other experimental research groups to plan and design magnetohydrodynamic dynamo experiments simulating the fluid flow topologies in planetary cores and stellar interiors more realistically. In particular the large-scale feedback of the dynamo magnetic field on a free bulk flow pattern in planetary cores is in the focus of such experiments. A survey of the respective experimental activities is given in the proceedings of Chossat, Armbruster, Oprea (2001), and in an article by Gailitis et al. (2002). This research target is beyond the capability of channelled sodium flows as realized in the Riga and Karlsruhe test facilities.

Nevertheless, even if of limited use for geo- and astrophysical application, we considered an experimental investigation of the back-reaction of a growing dynamo magnetic field on the velocity distribution to be of fundamental interest and worth to perform in the Karlsruhe test facility, since it may further elucidate the saturation mechanism in the trans-critical range. In another series of dynamo experiments we have addressed this problem that will be outlined in this article. The key-experimental issue in this context is the simultaneous measurement of the local sodium velocity in the channels of the test facility and the intensity of the local magnetic field in the vicinity of the velocity probes. This article is organized as follows: Section 2 recalls

briefly the principle design of the Karlsruhe test facility and outlines the specific instrumentation. The measured results for the magnetic field, and the local velocity in the axial flow channels are presented in section 3. In section 4 the experimental observations are discussed and some conclusions are drawn.

2. The test facility and its instrumentation

Stieglitz & Müller (1996) and Müller, Stieglitz & Horanyi (2004) described the Karlsruhe test facility in some detail. The test rig consists essentially of a cylindrical module which contains 52 channel type vortex generators connected to three independent sodium loops each of which is equipped with a MHD feed pump and a heat exchanger to ensure constant operational temperature during the experimental runs. The helical and axial channel flow in the vortex generators can be independently controlled by forced flow in the different sodium loops. (For more details compare the cited report and article.) The structure and the principle arrangement of the vortex generators is sketched in figure 1 together with essentials of the instrumentation and a coordinate system.

The sodium volumetric flow rate in each sodium loop was measured by electromagnetic flow meters outside the test module. The pressure drop across the module channel systems was determined by capacitance pressure gauges. The dynamo magnetic field was identified by two independent sensor systems. Four Hall sensors attached to a traversable prong moving in a borehole along the centre axis of the module were used to measure locally all the three components of the magnetic field. Two more Hall sensors are fixed at positions on the module's mantle (see figure 1). The transient phase of onset of dynamo action as well as the dynamic behaviour of

the magnetic field at constant supercritical operation could be measured through a set of sensor wire coils that are either threaded through the borehole in the module centre or are twined around the module equator as indicated schematically in figure 1. These sensor coils picked up time variations of the overall magnetic fluxes through planes of different orientation in terms of induced voltage time series depending on the spatial arrangement of the respective coils.

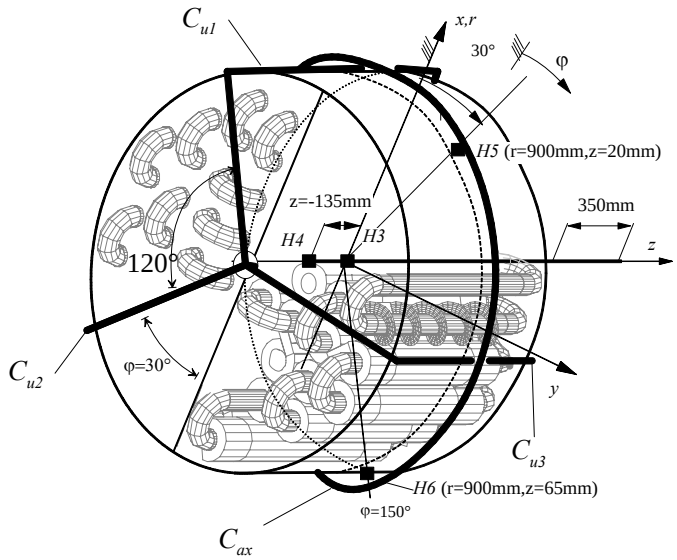

Figure 1: Technical sketch of the dynamo module and its instrumentation with Hall-sensors and flux sensors embedded in a coordinate system. H3: two Hall sensors to measure three field components B_x, B_y, B_z; H4: one Hall sensor to measure B_y; H5: one Hall sensor to measure two components Bz and the radial component B_r; H6: one Hall sensor to measure the radial component B_r; C_{ax}: sensor coil to measure the axial magnetic flux component Φ_z; C_{u1}, C_{u2}, C_{u3}: sensor coils to measure the azimuthal magnetic flux component Φ_φ.

The measurement of the local velocity in the channels of the dynamo module is crucial for studying the feedback of the dynamo magnetic field on the velocity. For that purpose we used so-called permanent magnet probes in an uncompensated or, more appropriate, a compensated design form. Two velocity probes were placed in axial channels of the module next to the axis of the cylinder as sketched in figure 2. A straight compensated probe was positioned with its tip in the centre of the channel. The other non-compensated probe has a bent form and is located with its tip close to the channel wall to sense the velocity overshoot near the exit of a flow return bent at the module's flat boundary. The specific measures for the location of each probe are given in figure 2. The measuring principle of these probes is based on Ohm's law in moving electrically conducting media. Employing this measuring principle in the environment of the dynamo magnetic field requires an evaluation procedure that eliminates the influence of the dynamo field from a measured voltage between electrical poles in the fluid.[1]

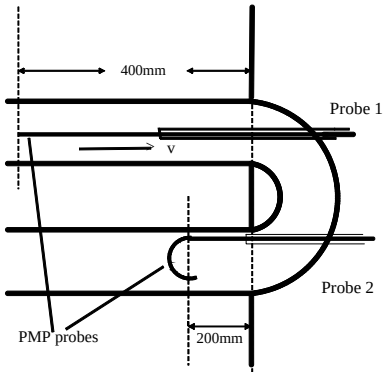

Figure 2: Sketch of the arrangement of two permanent magnet probes (PMP) in the axial channels of the vortex generators.

[1] The compensated permanent magnet probe has been developed originally by Knebel & Krebs (1994) to account for thermo electric effects when measuring velocities in non isothermal sodium flow.

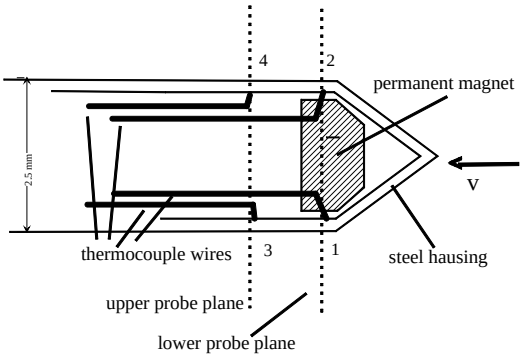

Figure 3: Sketch of the compensated permanent magnet probe (CPMP).

A sketch of the compensated permanent magnet probe (CPMP) is shown in figure 3. A miniature permanent dipole magnet of 2 mm in diameter is placed near the tip of a small stainless steel tube of 2 mm inner and 2.5 mm outer diameter. Two pairs of thermocouple wires are welded to the wall inside the tube, one pair in a plane cutting the small dipole magnet, the other pair in another plane in some distance (3 mm) downstream the first one. The attachment of the thermocouple tips at the tube walls with regard to the orientation of the magnetic dipole is such that a maximum induced voltage is recorded when liquid sodium bypasses the tip of the probe. At the uncompensated probe the second pair of thermocouples is missing otherwise the design is the same. The relationship between the velocity *u* parallel to the probe shaft, the induced voltage *E* between two thermocouple poles and the local intensity of the magnetic induction is given as $E \sim u \cdot B_{\perp}$ where $B_{\perp}$ is the component of the magnetic induction perpendicular to the electrical dipole formed by a pair of thermocouples. We may decompose the induced voltage *E*, the velocity *u* and the dynamo magnetic induction B_D in a mean and fluctuating component that reads as $E = \overline{E} + E'$, $u = \overline{u} + u'$, $B_{\perp} = B_{PM} + \overline{B}_D + B_D^{'}$ where B_{PM} is the contribution of the permanent

magnet to the overall magnetic induction at the probe tip. Inserting these relationships into the induction relationship and using simple averaging rules gives

$$\overline{E} \sim \overline{u}\, B_{PM} + \overline{u' B_D^{'}} + \overline{u}\, \overline{B}_D \ , \qquad (1a)$$

$$E' \sim u' B_D^{'} - \overline{u' B_D^{'}} + \overline{u}\, B_D^{'} + u' \overline{B}_D + u' B_{PM} \ . \qquad (1b)$$

These relationships hold for the measured voltage at the pair of thermocouples in plane 1 and plane 2 of the probe tip. Because of the short distance between the two planes, here 3mm, we may assume that the mean and fluctuating parts of the velocity and the induced dynamo magnetic field are the same in the two planes, i.e. $\overline{u}_1 = \overline{u}_2$, $u_1^{'} = u_2^{'}$, $\overline{B}_{D1} = \overline{B}_{D2}$, $B_{D1}^{'} = B_{D2}^{'}$. With these assumptions and applying relationships 1 to both planes of the sensor, we arrive after some algebra at the following expressions for the mean and fluctuating velocities

$$\overline{u} \sim \frac{\overline{E}_1 - \overline{E}_2}{B_{PM1} - B_{PM2}} \ , \qquad (2a)$$

$$u' \sim \frac{E_1^{'} - E_2^{'}}{B_{PM1} - B_{PM2}} . \qquad (2b)$$

Where B_{PM1} and B_{PM2} are the intensities of the magnetic induction of the permanent magnet in the respective measuring planes of the thermocouple dipoles. Introducing the ratio of the induction intensities $\alpha = B_{PM2}/B_{PM1}$ and a proportionality factor γ the evaluation of relationships 2a and 2b for the velocities to be measured by the CPM-probe read as

$$\overline{u} = \gamma \frac{\overline{E}_1 - \overline{E}_2}{1-\alpha} \ , \ u' = \gamma \frac{E_1' - E_2'}{1-\alpha} \ . \qquad \text{(3a,b)}$$

The values of the factor γ and the ratio α was determined from calibration measurements under sub-critical, i.e. non-dynamo active flow conditions. This is outlined in the appendix. In case of a non-compensated PM-probe an evaluation of the local velocity, using the measured induced voltage at the probe tip, can only be achieved if simultaneously the intensity of the mean dynamo magnetic field and its orientation with regard to the orientation of thermocouple dipole at the probe tip is known. The evaluation relationship for the mean velocity is then given as

$$\overline{u} = \gamma \frac{\overline{E}}{B_{PM} + \left|B_D\right| \sin \beta} \qquad \text{(4)}$$

Where β is the angle between the direction of the magnetic field and the orientation of the electrical dipole. We have indeed tried to conclude on the local mean velocity by measuring the intensity and orientation of the mean dynamo magnetic field in the vicinity of the probe tip. However, this evaluation procedure is affected with systematic errors mainly because the two relevant sensors, the Hall sensor and the PM-probe 2, were 0,17m apart from each other (the smallest achievable distance) for the particular measurement. We estimated the relative error of this systematic deficiency to amount to up to 20% for the strongest achievable dynamo activity but less than 3% for the pure hydrodynamic case. Therefore, we consider results based on this evaluation only as of qualitative nature. The details of this evaluation procedure are described in the appendix.

3. Results

3.1 The magnetic field

The components of the mean dynamo magnetic induction were recorded along the positive z-axis of test module employing the traversable Hall probes. For technical reasons requiring the coolability of the Hall sensors the probe could not be traversed beyond the centre of the axis to positions z<0. A typical measured distribution of the field intensity is shown in figure 4 for fixed flow rates $\dot{V}_c = \dot{V}_H = 111 m^3 / h$ in the axial and helical channels of the vortex generators. The data represent mean values averaged over time intervals between 1<Δt<3min. at a data recording frequency of 512Hz.

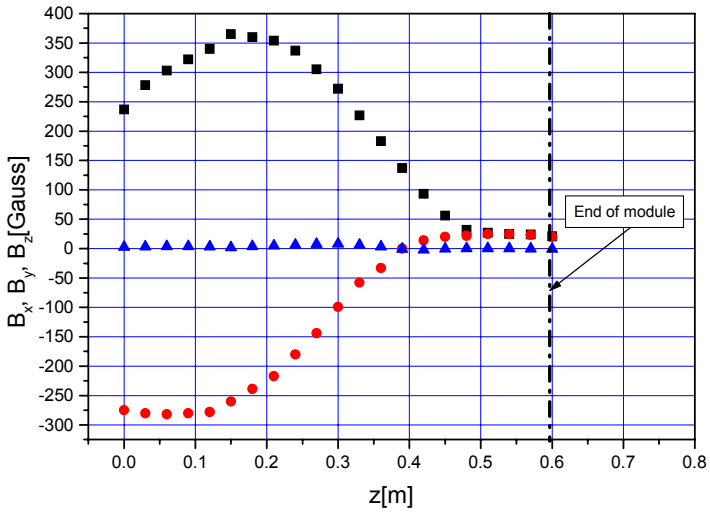

Figure 4: Measured components of the magnetic induction B_x (■), B_y (●), B_z (▲) along the module axis in the range 0 ≤ z ≤ 0,60 m for the volumetric flow rates $\dot{V}_c = \dot{V}_H =$ 111 [m^3/h].

Compared to previous measurements (see Müller et al. (2004)) the range of the recorded data has been doubled to the axial position z = 0.60m which even covers a

distance of 0.1m outside the module. As previously observed the location of the highest field intensity is not in, but only near the centre of the module and thus indicates a significant internal structural asymmetry with regard to a xy-plane through the centre (see figure 1).

Previous measurements have shown that the dynamo magnetic field is not stationary rather it fluctuates about its mean value with significant amplitude at all recordable time scales. This is seen in figure 5 which displays time series for the B_y and B_z components recorded in the centre of the module (fig.5a, b) by a Hall sensor, the axial magnetic flux component Φ_z (fig.5c) recorded by the sensor coil twined around the equator of the test module and the azimuthal magnetic flux Φ_φ (fig 5d) through a sensor coil threaded through the borehole along the z-axis and inclined by an angle of $\varphi = 30°$.

The presented records were made at the most intensive dynamo action that was technically achievable i.e. at equal volumetric flow rates $\dot{V}_c = \dot{V}_H = 115[m^3/h]$ in the supply loops.

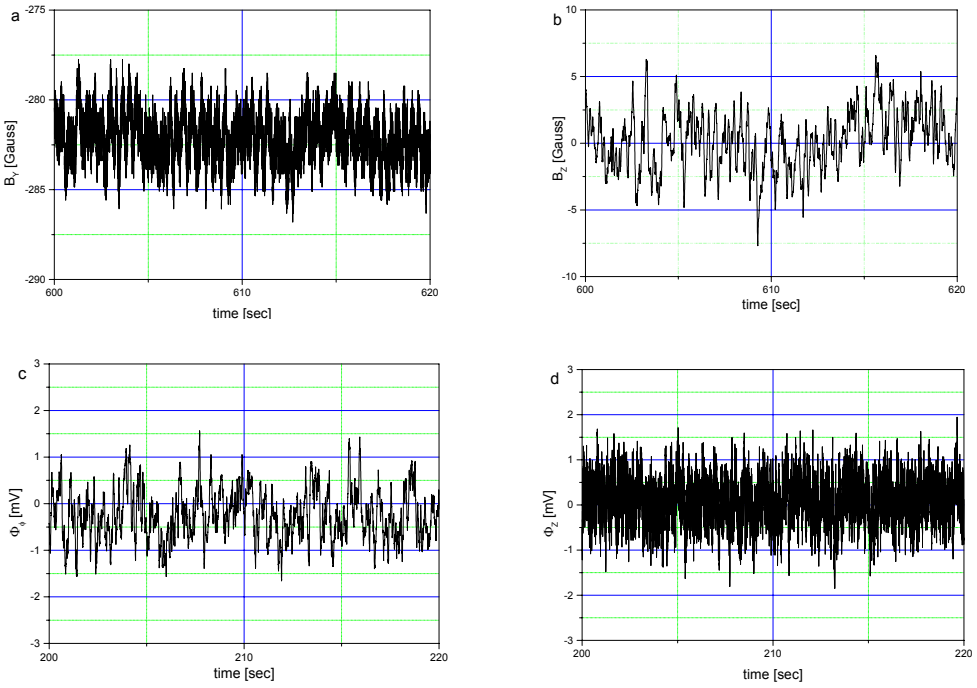

Figure 5: Typical time series recordings of the magnetic induction B_y (a) and B_z (b) measured with the Hall probe H3 at position z=0,075m (displayed in units [Gauss]) as well as the magnetic flux Φ_Φ (c) and Φ_z (d) measured at the sensor coil C_{u1} for the azimuthal magnetic flux and the sensor coil C_{ax} for the axial flux.(in units [µV]) Operational conditions: $\dot{V}_c = \dot{V}_H = 115\ [m^3/h]$.

More specific features of the field fluctuation may be identified from power spectral densities (PSD) associated with the time signals in figure 5. The respective PSD-functions are shown in figure 6.

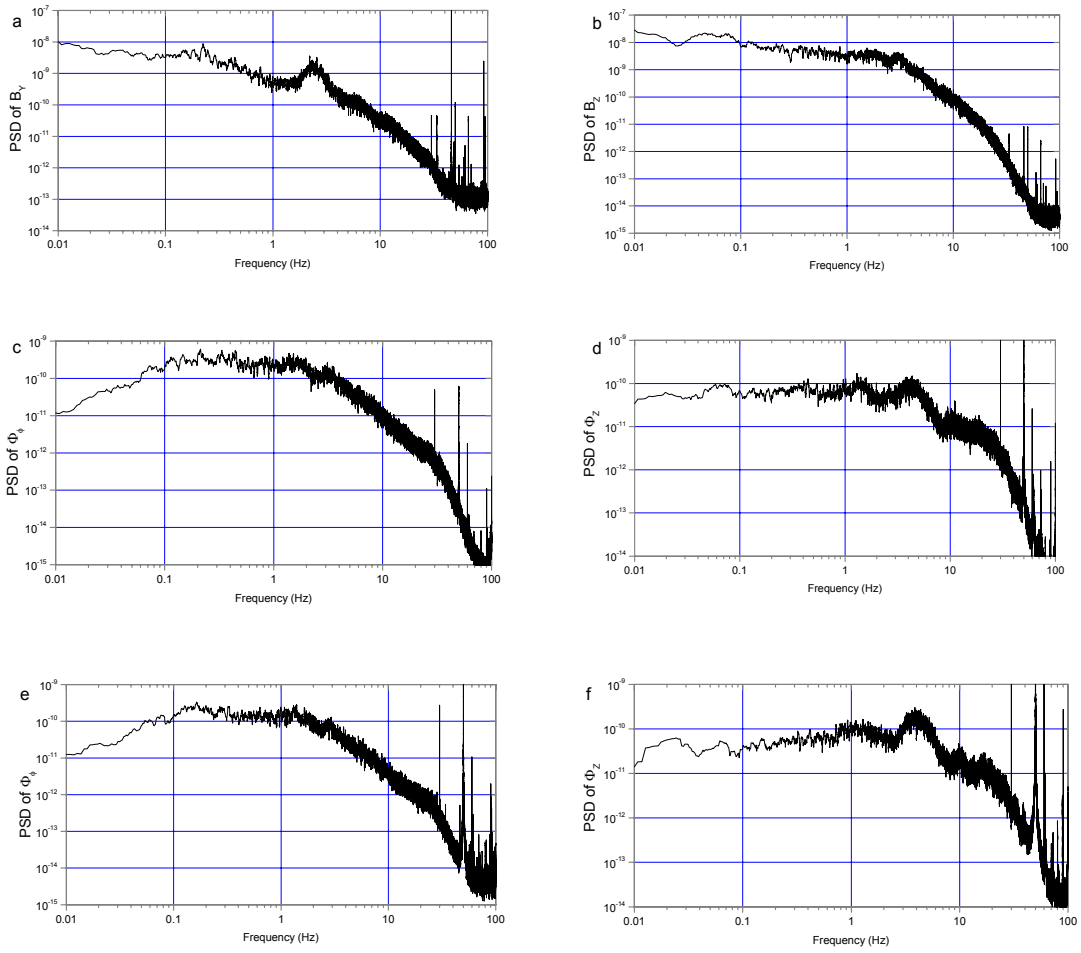

Figure 6: a, b, c, d) Power spectral densities (PSD) for the time series of figure 5 and e, f) PSD of the magnetic flux signal Φ_φ and Φ_z of the poloidal and equatorial sensor coil for the operational condition V_C=V_H= 105[m^3/h].

All spectra have in common the strong power reduction in the frequency range *3<f[Hz]<20* and an even steeper decrease of power for frequencies *f>20 Hz*. The power spectral density of B_y recorded by the Hall probe shows the characteristic broadband peak centred on the frequency $f \approx 2.8$ *Hz* that was already observed in previous experiments (Müller et al 2004) under the same operational conditions. The PSD-functions obtained from the recorded time-signals of the sensor coils show two more characteristic features in the flow frequency range: a) Another broad band peak

centred around a frequency of $f \sim 4\text{-}5Hz$ can be observed for the ϕ_z-signal which, in contrast to the peak in the PSD of the Hall sensor signal, does not noticeably change when the operational conditions change to lower flow rates as seen in figure 5f (see Müller et al. 2004). b) The PSD-function obtained from the azimuthal coils, sensitive to changes of the torroidal magnetic flux, exhibit a typical power plateau in an intermediate frequency range $0.1 < f[Hz] < 3$ moderately to the lower frequency range $f < 0.1Hz$ and strongly in the higher range $f > 3Hz$.

Furthermore, there is a significant cross-correlation between the different components of the magnetic field measured by Hall sensors at different positions but in moderate distance from each other. A typical cross-correlation function (CCF) is shown in figure 7 for the supercritical conditions $\dot{V}_c = \dot{V}_H = 112[m^3/h]$.

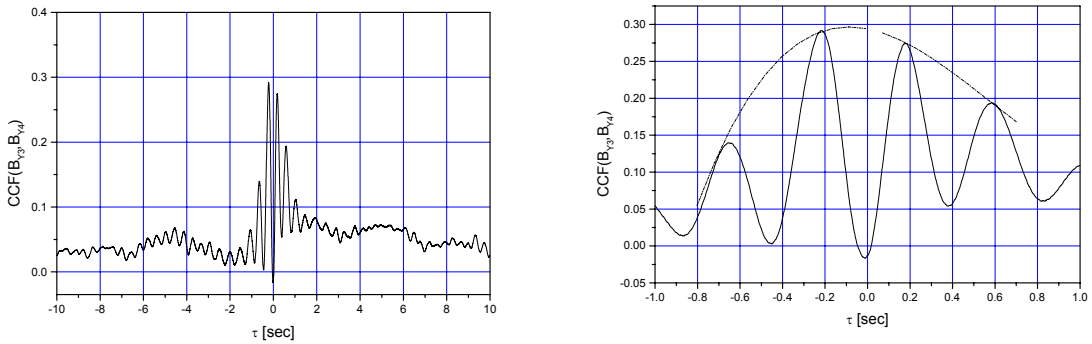

Figure 7: Cross-correlation functions for time signals of the B_y-components of the magnetic induction recorded by the Hall-probes at position H3 and H4; distance between the probes: d = 0,135 m.

The time signals of the B_y-components, recorded on the axis of the module at positions z = -0.06 m and z = 0.075 m, are correlated through a quasi-periodic fluctuation with a period of about $\tau \approx 0.4$ s. Likewise a delay time $\tau \approx 0.1$s may be identified from the graph by estimating the position of the maximum of an envelope to the oscillatory

CCF as Δt ≈ -0, 1s. These two effects may be interpreted by a perturbation wave package travelling at a group velocity of about 0,1 s.

3.2 Velocity characteristics due to the feedback of the dynamo magnetic field

Figure 8 presents evaluated data from signals recorded by the compensated PM-probe 1 and the uncompensated PM-probe 2.

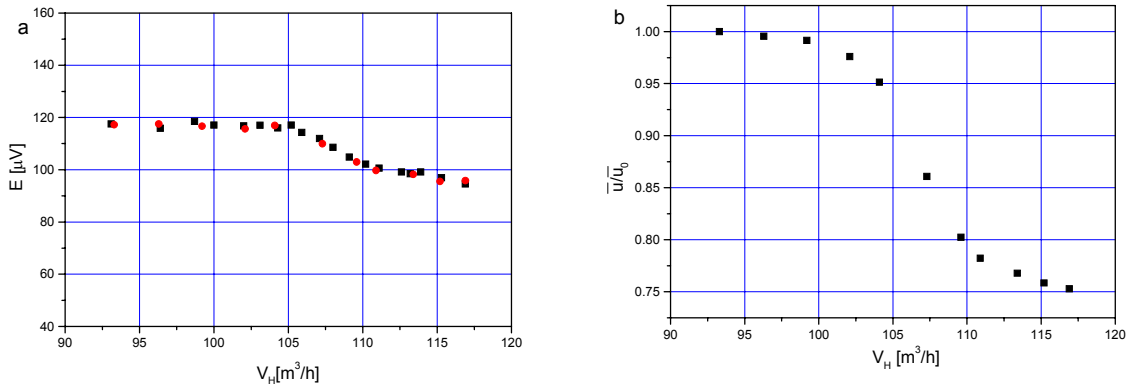

Figure 8: a) The measured compensated induced voltage from the permanent magnet probe 1 (CPMP) in the centre of an axial channel of a vortex generator next to the axis of the module as a function of the helical flow rates at a fixed axial flow rate of V_C=*105[m³/h].* According to calibration measurements the following relation holds: 1µV measured at the PMP corresponds to an axial local velocity variation $\Delta u = 3{,}19 \cdot 10^{-2}$ [m/s] (see appendix1). (Symbols ■, ● represent measurements on different days.)

b) The normalized axial velocity evaluated from data recorded by the uncompensated bent PM probe 2 and a near by Hall sensor (see figure 2 and appendix).

The graph in figure 8a shows the influence of the dynamo magnetic field on the local mean velocity in the centre of an axial channel at a position z = 0,075 m which corre-

sponds to a distance d = 0,565 m of the probe tip from the inlet cross section. The experiment was conducted at a fixed flow rate of $\dot{V}_c = 105[m^3/h]$ and for varying helical flow rates in the range $93 < \dot{V}_H \leq 118\ [m^3/h]$. For sub critical conditions, i.e. $\dot{V}_H < 105\ [m^3/h]$, the local velocity represented by the measured induced voltage is constant. Once dynamo action sets in at higher helical flow rates the velocity, i.e. the measured voltage, decreases first, but finally saturates at a lower level for even higher helical flow rates because of a strong influence of the dynamo magnetic field of the order of several hundred Gauss (see e.g. figure 4) in terms of Lorentz forces. The maximum velocity in the channel centre at sub-critical conditions is reduced by 17% to its plateau value at the distinctly supercritical state.

We observed a similar effect on the local velocity at the other, non-compensated PM-probe 2 under similar operational conditions, i.e. at a constant axial volumetric flux of $\dot{V}_c = 105\ [m^3/h]$ and varying helical flow rates. The evaluated effective voltage, which is proportional to the local axial velocity at the tip of the second probe, is plotted in figure 8b. Although this graphs is affected by uncertainties of about 20% at the highest and by less then 3% at the lowest helical flow rate in the evaluation procedure, as outlined in the appendix (see in the appendix relationship A2), the data sequence clearly indicates a transition from a higher to a reduced velocity level when the intensity of the dynamo magnetic field increases with increasing helical flow rates. The relative variation of the velocity between the two levels is larger than that observed at the first probe. This seems to be reasonable as the bent PM-probe 2 (see figure 2) senses the velocity excess at the outer edge of the return flow bent connecting adjacent axial channels (see figure 1) which is less affected by the acting Lorentz forces.

The response of the dynamo magnetic field on the velocity fluctuations can be identified from the RMS-values of the compensated time signal recorded at probe 1. A se-

quence of RMS-data for sub critical and supercritical flow conditions are plotted in figure 9 for equal flow rates in the channel systems.

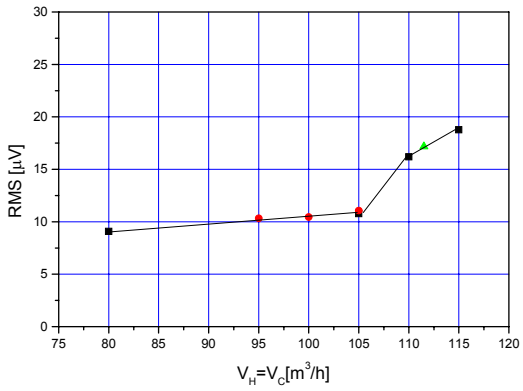

Figure 9: The evaluated RMS-values for the axial velocity fluctuations as a function of the volumetric flow rates for conditions of equal helical and axial flow rates, •, ▲, ■ experimental data recorded on different days, — fitting line.

The data were evaluated from recordings of 20 minutes at a data acquisition rate of 512 per second and for equal axial and helical flow rates. At sub-critical flow rates, i.e. $\dot{V}_c = \dot{V}_H < 105\ [m^3/h]$ we observe a weak linear increase of the RMS values. When dynamo action sets in for $\dot{V}_c = \dot{V}_H \geq 105\ [m^3/h]$ the growth rate of the RMS-values becomes suddenly larger, but levels off for even higher volumetric flow rates as is indicated by the fitting line through the data points. The data sequence thus seems to reflect the phase transition from the hydrodynamic to the dynamo state and the saturation of dynamo action due to the feedback of the magnetic field on the velocity distribution.

For representative subcritical, near critical and supercritical states the power spectral densities of the compensated velocity signal at probe 1 are shown in figure 10.

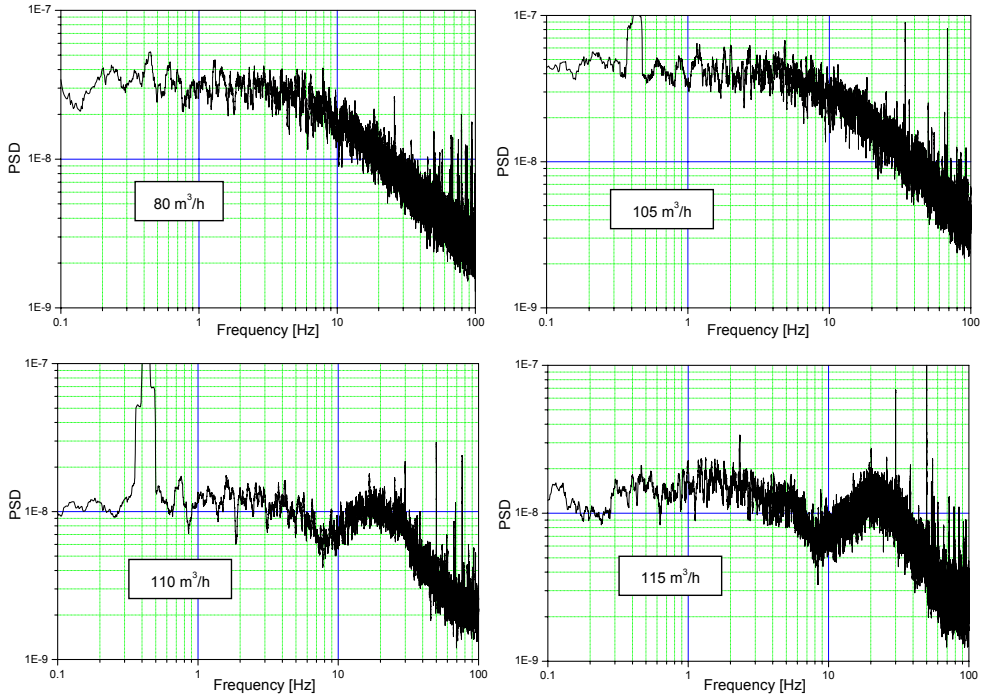

Figure 10: Power spectral density (PSD) for the velocity signal from the compensated permanent magnet probe (CPMP) recorded for sub critical ($\dot{V}_c = \dot{V}_H = 80$ [m³/h]), near critical ($\dot{V}_c = \dot{V}_H = 105$ [m³/h]) and supercritical ($\dot{V}_c = \dot{V}_H = 110$ [m³/h]; $\dot{V}_c = \dot{V}_H = 115$ [m³/h]) operational conditions.[2]

As characteristic features we find: The general level of the PSD-function increases only slighly in the sub critical and near critical range ($\dot{V}_c = \dot{V}_H = 80$ [m³/h], $\dot{V}_c = \dot{V}_H = 105$ [m³/h]), but decreases noticeably compared to that in the supercritical range ($\dot{V}_c = \dot{V}_H = 110$ [m³/h], $\dot{V}_c = \dot{V}_H = 115$ [m³/h]). Furthermore, at supercritical conditions spectral power is shifted from the lower to the higher frequency range. As a consequence, a stronger decay of power occurs in the observable final range which indi-

[2] The power peaks in the low frequency range at $f \approx 0{,}4Hz$ of the spectra for flow rates *105 and 110[m³/h]* are not physically reasonable and are attributed to an unidentified experimental perturbation.

cates a significant increase of the magnetohydrodynamic dissipation. There is also an intermediate frequency range 5<f<10 Hz of reduced power at super critical conditions. A power accumulation adjoins this power suppression as seen by the broad bend peak around a frequency $f \approx 20$ *Hz.* This observation indicates a obviously non-uniform, selective damping mechanism for the velocity fluctuations in the higher frequency domain under the influence of the dynamo magnetic field.

Another challenging aspect of dynamo action is the mutual influence between fluctuations of the magnetic field and the velocity. We investigated this issue by cross correlating the time signals of the compensated PM-probe 1 with those of the Hall- and coil-sensors for different components of the magnetic induction and flux respectively and for various operational states. We found relevant correlations between the signals only for short distances between the locations of the probes, for short time scales of the order less than 1 s and under conditions for the largest technically feasible dynamo magnetic fields of several hundred Gauss. A typical example for a cross-correlation between the time signal for the velocity from PM-probe 1 at a position x=0.1 m, y=0.1 m, z=0.075 m and a signal of the B_z-component from a Hall-sensor at position x=0, y=0, z=0.075 m is shown in figure 11.

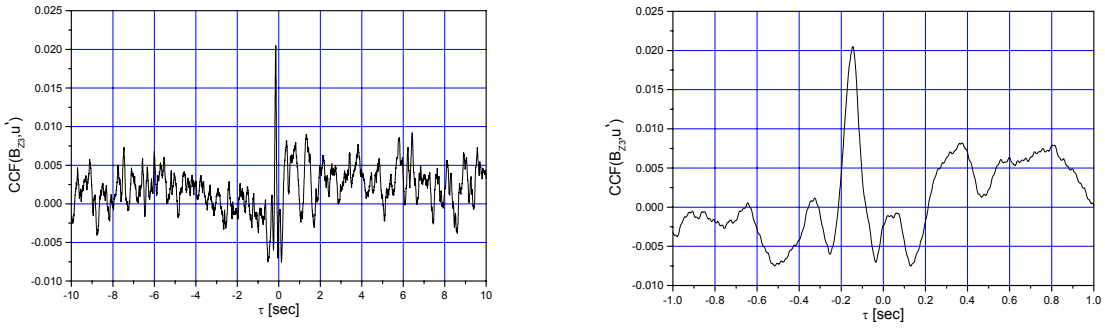

Figure 11: Normalized cross-correlation function (CCF) of the velocity signal recorded by the compensated permanent magnet probe at position (0.1, 0.1, 0.075 m) and the signal of a Hall probe for B_z at position (0, 0, 0.075 m). The CCF is presented for two temporal reductions *(-10<t[s]<10)* and *(-1<t[s]<1).* Operational conditions: $\dot{V}_c = \dot{V}_H =$ 115 [m^3/h].

The operational conditions were $\dot{V}_c = \dot{V}_H = 115\ [m^3/h]$. The correlation graph shows two characteristic features: a) a small, nevertheless, distinct 2% correlation of a quasi-periodic fluctuation of a period of about $\tau_P \approx 0.2$ *s*, b) a time delay of $\tau_d \approx -0.15$ *s*. According to Bendat & Piersol (1986) the quality of the CCF in figure 11 may be associated to a narrow band random noise signals. The same quality of correlation was also observed for a state of operation with $\dot{V}_c = \dot{V}_H = 112\ [m^3/h]$, however, not for even lower flow rates. No significant correlations could be identified between the other two components of the magnetic induction B_x, B_y and the velocity from the corresponding time signals under the same flow rate conditions.

The cross-correlations between the time signals of the coil sensors (see figure 1) and the PM-probe 1 showed similar features. Two typical examples for an axial and azimuthal magnetic flux are presented in figure 12.

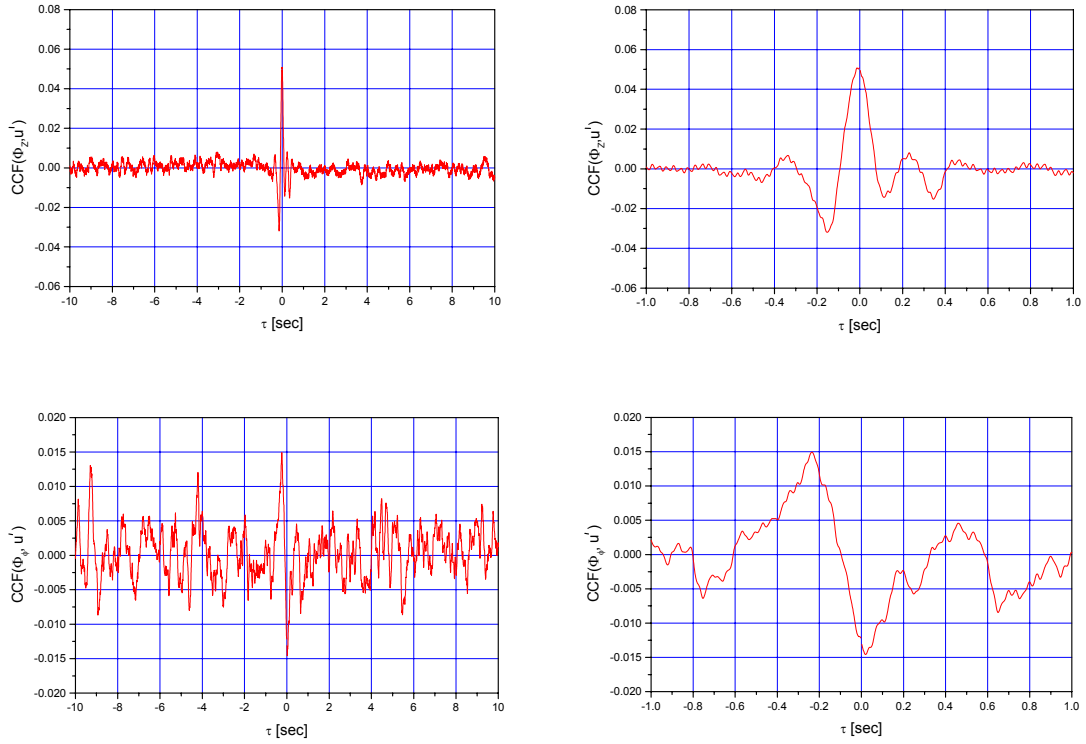

Figure 12: Cross-correlation functions (CCF) of the velocity signal recorded by the compensated permanent magnet probe 1 at position (0.1, 0.1, 0.075 m) and signal of the coil flux sensors C_{ax} (a) and C_{u1} (b) for the axial and azimuthal magnetic flux components. Each CCF is presented for two different time intervals *(-10<t[s]<10)* and *(-1<t[s]<1).* Operational conditions: $\dot{V}_c = \dot{V}_H = 115\ [m^3/h]$.

The operational conditions were the same as in figure 10. The 'equator'-coil measured the axial flux Φ_z. The azimuthal flux signal Φ_φ was recorded by a coil in a plane inclined by an angle of 30° to the (x, z)-coordinate plane (see figure 1). In figure 12a a correlation of about 5% is seen between the axial magnetic flux and the velocity in the axial channel. Moreover, there is a strongly dampened, quasi-periodic correlation signal for a time interval $|\Delta t| < 0.4$ s with a period of about $\tau \approx 0.2$ s in accord with the observation for the correlation between the Hall- and the CPM-probe signals in

figure 11. A noticeable time delay does not exist in contrast to the Hall- and CPM-probe signals. A significant correlation between the measured azimuthal magnetic flux and the axial velocity cannot be identified from figure 12b. This is in accordance with the observation for correlations between the B_y, B_x-components and the axial velocity.

4. Discussion

4.1 Properties of the magnetic field

The more detailed measurements of the magnetic induction on the module axis can now be compared with the shape functions for the whole axial range calculated by Tilgner (2003) and Rädler et al. (2002) within the scope of a kinematic dynamo model. Here we show the results of Tilgner in figure 13.

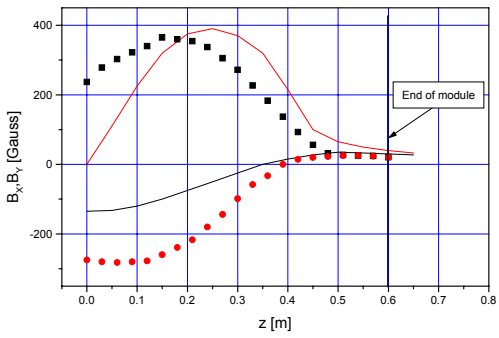

Figure 13: Comparison of measured components of magnetic induction B_x, (■) B_y (●) and calculated values (—) by Tilgner (2003).

(For a comparison between theoretical results of Rädler et al. (2002) and our earlier measurements see Müller et al (2004).) The graph confirms our conjecture from previous experiments (Müller et al. 2004) that the technical performance of the test

module gives rise to an intrinsic non-symmetry of the magnetic field inside the module compared to the calculated "symmetric" shape functions. This is best evidenced by the shift of the measured and calculated maximum locations of the intensities and by the finite value of B_x at $z=0$ There is a good qualitative agreement between the measured and calculated field intensity in the vicinity of the module's flat wall and further outside.

The time series records of the magnetic induction and the magnetic flux displayed in figure 5 as obtained from two independent sensor systems, the Hall sensors and the coil sensors, show at first glance similar stochastic characteristics when comparing the corresponding poloidal and toroidal components. The associated power spectra in figure 6, however, reveal striking differences. The specific features of the power spectral densities of the time signals recorded by the Hall sensors near the centre of the module (figure 6a,b) match very well with evaluations of previous measurements (Fig. 21 in Müller et al. 2004) and were discussed at length. Nevertheless, we would like to point out again that the broad band peak centered around the frequency $f \approx 2.8\ Hz$ in the PSD-function of the B_y-component in figure 6 shifts to lower frequencies for decreasing intensities of the measured magnetic field, i.e. for lower volumetric flow rates. We found this power peak at $f \approx 1\ Hz$ for volumetric flow rates $\dot{V}_c = \dot{V}_H = 105\ \left[m^3/h\right]$ in agreement with our earlier measurements. We conjectured previously, and still do, that this effect reflects a resonant interaction of Alfven fluctuations at the smallest length scale of the test module, i.e. at twice the diameter of a vortex generator.

We observe a distinct broad bend power peak of a similar kind also in figure 6d in the power spectral density of the signal from the equatorial coil sensing the magnetic

field fluctuations along the module axis. The peak is centered around a frequency of $f \approx 4\text{-}5\ Hz$. However, contrary to measured local signals by Hall sensors, the location of the "power hill" in the frequency domain does not change noticeably if we reduced the operational volumetric flow rates, e.g. to $\dot{V}_c = \dot{V}_H = 105\ \left[m^3/h\right]$. This can be seen from figure 6f. We suggest that the location of the power peak is not governed by the intensity of the magnetic field but originates from hydrodynamic fluctuations of the swirling flow in the vortex generators that stretches and transports the mean magnetic field lines. A time scale in accord with this idea is given by the injection frequency of hydrodynamic helicity into the system. This may be defined e.g. as $f_{in} = \frac{\overline{u}_H}{a \cdot \pi}$ where $\overline{u}_H$ is the mean velocity in the helical channels, *a* the diameter of the vortex generator (see table in the appendix of Müller et al. (2004)). For our specific cases this results in values $f_i \approx 4.7\ Hz$ for volumetric flow rates $\dot{V}_c = \dot{V}_H = 115\ \left[m^3/h\right]$, and in $f_i \approx 4.2\ Hz$ for the flow rates $\dot{V}_c = \dot{V}_H = 105\ \left[m^3/h\right]$. We consider this as a reasonable estimate with regard to the rough assumptions for the velocity distribution in the helical channel. Using the mean velocities in the channels, which are of the order of *3-4 [m/s]*, directly would result in to a one order higher estimated frequency (compare table 1 in Müller et al. 2004).

The power spectrum evaluated from signals recorded by the poloidal sensor coils, as depicted in figure 6c, shows a characteristic accumulation of power in the range of frequencies $0.1<f[Hz]<1.2$ with a strong power decay to higher and a moderate power reduction to lower frequencies. We may display this observation also in the wave number space by using Taylor's hypothesis and a typical velocity of the system, say the mean velocity in the axial channels which is typically $\overline{u}_{ax} \approx 4\ [m/s]$. The power containing wave number range would than be $0.2<k[m^{-1}]<1.9$

and the associated range of wave lengths would be $3<\lambda[m]<30$. This means the main energy of the dynamo magnetic field is being accumulated in the large-scale field components.

All the displayed spectra in figure 6 have in common the strong decay in the dissipative range of frequencies beyond the Kolmogorov frequency $f_{K\lambda}$ based on the magnetic diffusivity which we evaluated previously (see Table 1 in Müller et al. 2004) and which varies for the cases considered between $9<f_{k\lambda}[Hz]<15$.

It is not surprising that significant cross correlations exist between components of the magnetic field measured at different but not too distant locations as demonstrated in figure 7. There are at least two possible mechanisms for spatial correlations a) the radiative energy transport by Alfven waves and b) the convective energy transport by the fluid flow in the channels. The first one is certainly limited to short distances because of the strong Joule damping of these waves in liquid sodium. The rate of correlation may be expected to be weak even for short distances.

The display of the cross correlation functions (CCF) in figure 7 shows a relatively strong correlation of 30% between the fluctuations of B_y-components measured at locations on the module axis as outlined in section 3. The signals are associated mainly with random fluctuations. However, the correlation functions show a mean period of $\tau \approx 0.4\ s$ that is compatible with the observed frequency peak in PSD-function of the B_y-component in figure 6a. Moreover, a delay time of $\tau_d \approx 0.1$ [s] seems to exist which may be estimated from the location of the maximum of an envelope to the fluctuating and dampened CCF in figure 7b. This delay time is compatible with the assumption that a field disturbance within the helical flow domain is transported by the axial component of the helical velocity to the location of the second Hall

sensor. The transport velocity is associated with the volumetric helical flow rate $\dot{V}_H = 115\ \left[m^3 / h\right]$ and is calculated roughly as $u_{trans.Hel.} \approx 1{,}16\ m/s$.

4.2 The feedback of the magnetic field on the velocity

The decrease of the velocity with increasing helical flow rates, as seen in figure 8, must be interpreted by a transition of an ordinary turbulent velocity profile in a circular channel to a slug-type MHD velocity profile under the influence of the increasing intensity of the mean magnetic field. This magnetic field is essentially perpendicular to the channel direction and induces Lorentz forces to generate velocity redistributions. From MHD-textbooks (see e.g. Branover(1978), Moreau (1990), Müller & Bühler (2001)) it is known that a balance between pressure and Lorentz forces governs the channel flow at Hartmann numbers of several hundred and that slug type velocity profiles occur. For figure 8 the achieved maximum local magnetic field intensities were a) *479 [Gauss]* at a helical volumetric flow rate $\dot{V}_H = 118\ \left[m^3/h\right]$, b) *379 [Gauss]* at a helical flow rate $\dot{V}_H = 117\ \left[m^3/h\right]$ which corresponds to Hartmann numbers of *Ha=600* and *480* respectively (for the definition of the Hartmann number we refer to table 1 of Müller et al. 2004). This is a range where the core-flow, i.e. slug flow approximation holds for MHD-channel flow. The saturation behaviour of the velocity in figure 8 for high Hartmann numbers is thus obvious within the scope of an asymptotic MHD core-flow model. We mention here explicitly that the 17% decrease of the local velocity, measured by the CPM-probe 1 in the channel centre (see fig. 8a), is in fair agreement with the relationship of the maximum turbulent velocity in a fully developed turbulent pipe flow and the associated mean flow which is $\overline{u} = 0.837\, u_{\max}$ (see e.g. Schlichting 1958) and thus corroborates our explanations for the MHD-saturation process.

At first glance it is surprising that the velocity fluctuations and as their measure the RMS-values grow beyond the level of ordinary turbulence fluctuations under the influence of dynamo action, as figure 9 indicates. One could have speculated that be-

cause of Joule dissipation due to the dynamo magnetic field the fluctuation were dampened instead, at least in the channel centre. This has been observed for fully developed liquid metal pipe flow under the influence of a homogeneous external magnetic field (see also the above cited text books on MHD). In our experiment such clean conditions are not available. On the contrary, the channel flow is not fully developed only 6 pipe diameters downstream of a 180° bend and is contaminated by secondary flows in form of Dean vortices originating from the bent. Moreover, the flow enters a twisted, inhomogeneous magnetic field (see figure 4) that enforces an additional swirl flow interfering in a complex manner with the remnant Dean vortices. Thus, there are some arguments for an augmented turbulence level in the duct confining the axial flow under dynamo action. The sub-linear increase of the MHD-turbulence level, seen in figure 8b, seems reasonable in the light of a trans-critical bifurcation process that we encounter with the onset of dynamo action (see Müller et al. 2004).

Further insight into the back reaction of the magnetic field on the velocity fluctuations is obtained from the PSD-functions in figure 10 for sub-, near- and super-critical flow conditions. Assessing the technical quality of the PSD-functions in figure 10, we must realize that the power spectra are affected by significant, yet unidentified noise as the observable power reduction is only one decade in the relevant frequency range *0.1<f[Hz]<100.* Nevertheless, as a characteristic physical feature we see, that the power level in the low frequency range *0.4<f[Hz]<5* increases slightly from the sub-critical to the near-critical range ($\dot{V}_c = \dot{V}_H = 80\ \left[m^3/h\right]$, to $\dot{V}_c = \dot{V}_H = 105\ \left[m^3/h\right]$) but, compared to that, decreases in the super-critical range ($\dot{V}_c = \dot{V}_H = 110\ \left[m^3/h\right]$ to $\dot{V}_c = \dot{V}_H = 115\ \left[m^3/h\right]$). The power decay in the high frequency range *10<f[Hz]<100* fol-

lows fairly well a f^{-1} power law in the sub- and near-critical range and a $f^{-1.5}$ power law in the supercritical range. For fully developed turbulent pipe flow we expected, as outlined in Müller et al (2004), the Kolmogrow (1941) spectral distribution $E_f^V \sim f^{-5/3}$ for the inertial sub range at sub critical condition and a generalized (Biskamp (1993) Iroshnikov (1963) Kraichnan (1965)) energy spectrum for correlated MHD-turbulence in the form $E_f^V \sim f^{-m}$ with $3/2<m<3$. This is not the case for the hydrodynamic turbulence in our axial channel flow. For the magnetohydrodynamic turbulence only the lower limit of the generalized power law seems to have been realized. Moreover, our speculation to find the special spectral behaviour of velocity-turbulence under the influence of magnetic fields in the inertial-dissipative range say $20<f[Hz]<100$ as observed by Alemany et al. (1979) and Messadek & Moreau (2002) is not substantiated by the PSD-functions in figures 10c,d. We attribute this deficit mainly to the inadequate resolution of our probe in the high frequency range f>10 Hz and a too large signal to noise ratio of about *10* of the PM-probe 1 measuring chain. As a consequence, our former interpretations (Müller et al. 2004) of the observed strong spectral power decay of the magnetic energy, as displayed once more in the PSD-graphs in figure 6, cannot be based on our present experimental findings. Further experiments on MHD-turbulent flow under supercritical dynamo conditions are needed to clarify this issue.

The evaluations of the spatial cross-correlations between the velocity and magnetic field fluctuations presented in figures 11 and 12 show a distinct preference for an interaction of the co-oriented axial velocity and induction components u_z and B_z. This holds for the time series recorded by Hall- and the coil flux sensors. This may be interpreted as coherence between the axial velocity fluctuations and the stretching of mean radial magnetic lines of force by just these velocity fluctuations. The quasi-

periodic character of this coherency at a period of roughly $\tau \approx 0.2\ s$ underlines the hydrodynamic origin for this observation. This time period is compatible with the injection frequency for the hydrodynamic helicity into the system referred to above. The readable delay time between the correlated signals in figure 11b is $\tau_d \approx 0.15\ s$. Two transport mechanisms for the magnetic field offer an explanation for the observed delay time of the cross-correlation, namly Alfven waves and magnetic diffusivity. For our specific arrangement of the two probes the distance between them was *0,14 m.* The Alfven velocity based on the measured intensity of the mean magnetic field is $v_A \approx 1[m/s]$. This corresponds to a transport time of *0.14 s* for an Alfvenic fluctuation to travel between the two sensors, a value very close to the measured delay time of *0,15 s.* If we choose diffusion, described by the magnetic diffusivity $\lambda=0,1[m^2/s]$, as the governing transport process between the sensors, then this would result in a delay time of *0,2 s*, a value slightly higher than the observed one. Considering the two possible explanations and the closeness of the derived relevant transport times, the present data base does not provide a conclusive preference to one of them. The governing transport process for the fluctuatons of the magnetic field under supercritical dynamo conditions needs, therefore, further investigations.

The fact that we could not detect any significant delay time from cross-correlation measurements employing the PM-probe 1 and the equatorial coil sensor must be attributed to integrating effect of the coil sensor with regard to the flow in all 52 helical channels having a vanishing overall hydrodynamic helicity.

5 Conclusions

The presented experimental results complement and extend previous experimental investigations (Müller et al. 2004) in two respects.

Extending the measurements of the magnetic field components along the test module axis from the centre to a distinct location outside of the module specified furthermore the properties of the mean dynamo magnetic field. The measured data indicate an intrinsic non-symmetric field distribution in the real test module compared to calculated data obtained for an ideal symmetric test. The dynamic behaviour of the magnetic field was explored in addition by a signal analysis of time series for the azimuthal and axial dynamo magnetic flux obtained from sensor coils. The power spectra of the azimuthal flux show a power accumulation in an intermediate low frequency range that corresponds to large spatial scales of the magnetic field. The power spectra of the axial flux reveal the injection of mechanical helicity into the system by a power peak at a frequency that corresponds to the turn around time of the flow in the helical channels.

The back reaction of the dynamo magnetic field on the velocity distribution in the axial channels of the test module was analysed with the help of two permanent-magnet-potential-probes. The evaluation of the mean values of the probe signals indicates a transition of an ordinary turbulent pipe flow velocity profile into a magneto-hydrodynamic slug flow profile for increasing dynamo intensities. The measured local turbulent intensities of the velocity increase with the onset of dynamo action but exhibit a trend to saturation at pronounced super-critical conditions. This contrasts at first glance the common experience that turbulent fluctuations are dampened in fully developed MHD-channel-flow due to the additional Joule dissipation. However, the selective damping of the inhomogeneous dynamo mean magnetic field on velocity

perturbations downstream the 180° bend leads to a different observation. A significant cross-correlation exists between the time signals of the axial component of the dynamo magnetic field and the velocity in the axial channels for short spatial separations of the sensors. It is suggested that this interaction is caused by the axial convective transport of perturbations of the mean magnetic field generated by the helical flow components in the vortex generators.

Acknowledgement: The authors gratefully acknowledge the benevolent support by the director of the Institute for Nuclear- and Energy Technologies, Professor Schulenburg, during the preparation and the performance of the concluding dynamo experiments.

They owe great thanks to D. Schlindwein and his technical staff for their careful preparation of the tests and the operation of the dynamo test facility. Moreover, they thank their colleagues Dr. L. Bühler and Dr. L. Krebs for their critical comments on a first draft of this report.

References

Alemany, A., Moreau, R., Sulem, P.L. & Frisch, U., 1979:
Influence of an external magnetic field on homogeneous MHD turbulence. J. Mec. 18, 277-313.

Bendat, J. S. & Piersol, A. G. 1986 Random Data, Analysis and Measurement Procedures, Wiley-Interscience Publication.

Biskamp, D., 1993:
Nonlinear Magnetohydrodynamics, Cambridge University Press.

Branover, H., 1978:
Magnetohydrodynamic Flow in Ducts. John Wiley & Sons, New York

Busse, F.H., 2000:
Homogeneous dynamos in planetary cores and in the laboratory. Ann. Rev. Fluid Mech. 32, 838-903.

Cardin, P., Brito, D., Jault, D., Nataf, H.-C., Masso, J.-P., 2002 Towards a Rapidly Rotating Liquid Sodium Dynamo Experiment. Magnetohydrodynamics 38, 177-189.

Rädler, K.H., 1999 From the Sun to the Great Attractor. Lecture Notes in Physics, Springer, Berlin

Iroshnikov, P.S., 1963:
Turbulence of a conducting fluid in a strong magnetic field. Sov. Astron. 7, 566-571.

Knebel, J. U., Krebs, L. 1994 Calibration of a miniature permanent magnet flow meter probe and ist application to velocity measurements in liquid sodium. Exp. Thermal Fluid Sci. 8, 135-148.

Kolmogorov, A. N. 1941 Local structure of turbulence in an incompressible fluid at large Reynolds numbers. Dokl. Akad. Nauk. SSSR 30, 299-303.

Kraichnan, R.H., 1965:
Inertial range spectrum in hydromagnetic turbulence. Phys. Fluids 8, 1385-1387.

Messadek, K., & Moreau R. 2002 An experimental investigation of MHD quasi-two-dimensional turbulent shear flow. J. Fluid Mech. 456, 137-159.

Moreau, R. 1990 Magnetohydrodynamics. Kluwer Academic publishers, Dordrecht.

Müller, U. & Bühler, L. 2001 Magnetofluiddynamics in Channels and Containers. Springer, Heidelberg.

Müller, U., Stieglitz, R., Horanyi, S., 2004:
A two-scale hydromagnetic dynamo experiment. J. Fluid Mech. 498, pp. 31-71.

Rüdiger, G., Hollerbach, R. 2004 The Magnetic Universe. Wiley-VCH

Schlichting, H., 1958:
Grenzschicht-Theorie, G. Braun, Karlsruhe.

Stieglitz R. & Müller, U. 1996 GEODYNAMO: Eine Versuchsanlage zum Nachweis des homogenen Dynamoeffects. Wissenschaftlicher Bericht FZKA 5716.

Appendix

The calibration and testing of the permanent magnet probes (PMP) was done at fully installed conditions and for sub critical flow rates i.e. without dynamo action. The compensated PM probe was located in the centre of an axial channel at a distance of *l = 0,56* m from the exit of a return bent.

For several fixed volumetric flow rates the signals of the induced electromotoric force E was recorded from the ends of the two pairs of thermocouple wires of the probe (see fig. 3). (The volumetric flow rates in the axial channels of the module were measured by EM-flow meters outside the test module as described by Stieglitz & Müller (1996)).

A typical calibration record for two pairs of alumel thermocouple wires in a plane 1 and 2 of the PM-probe 1 is given in figure A.1

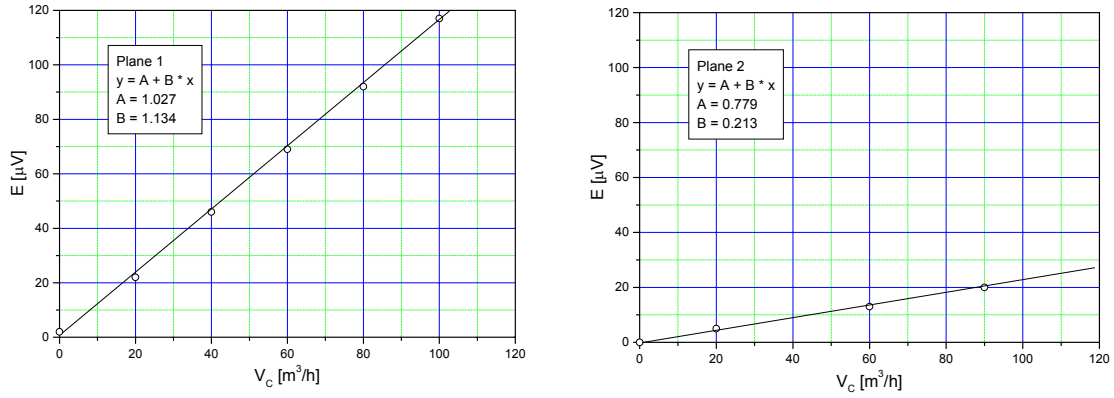

Figure A1: Calibration graph correlating induced voltages of PM probe (E) and volumetric flow rates in the axial channels.

There is a linear relation between the measured voltage E and the volumetric flow rates in the form $E = A + B\ \dot{V}_c$, where A defines the offset and B is the calibration

factor. From several calibration runs we found for the parameters of the alumel wires in plane1: B_1 = *(1.114 ± 0,02) [µV/(m³/h)].* The respective value for the alumel wire pair in plane 2 is: B_2 =*(0.210 ± 0,003) [µV/(m³/h)].* The estimated inaccuracy (caused by the PM probe sensor via electrical amplifier, and the volumetric flow detection) is less than 5 %. Assuming that the channel flow is fully developed in the centre of the channel we may use the relationship $\bar{u} = 0.837\ u_{max}$ between the average velocity and the maximum velocity for turbulent flow in a circular pipe (see e.g. Schlichting (1958) to correlate *B* even to the local mean velocity at the location of the probe tip.

The offset value that is primarily caused by the status of the measuring chain varied significantly between the different runs. No uniformly valid value could be determined by calibration tests and thus had to be evaluated specifically in separate experiments. Introducing the offset corrected measured values for electromotoric forces in plane 1 and plane 2 into equation 2a and using the calibration factors B_1 and B_2 we obtain for the volumetric flow rate sensed by the compensated PM-probe in the centre of the axial channel (diameter d=0.1 m)

$$\dot{V}_c = \left[m^3/h\right] = \frac{1}{B_1}\,\frac{\overline{E}_1 - \overline{E}_2}{(1 - B_2/B_1)} = 1{,}10\ (E_1 - E_2)\,\frac{\left[m^3/h\right]}{\left[\mu V\right]} \qquad \text{(A1)}$$

Assuming fully developed turbulent channel flow and relating the volumetric flow rate to the average channel velocity (with *1 [m³/h] ÷ 3,55 10⁻² [m/s]*) this yields for the maximum velocity in the channel centre

$$u_{max}\ [m/s] = 4.67 \cdot 10^{-2}\ (E1 - E2)\ \frac{[m/s]}{[\mu V]}\ . \qquad \text{(A2)}$$

The measurement of the velocity with the help of the compensated permanent magnet probe is flawed with errors originating from the measuring chain for the induced voltage at the probe tip and from variations in the power control of the pumps in the supply loops. The former errors are negligibly as the effective spatial resolution of the probe tip is of the order of 4mm corresponding to a frequency resolution of flow perturbations up to 1kHz and the sensitivity of the measuring chain is $\Delta E \approx 0,1 \mu V$. The uncertainty in the power control of the MHD-pumps amounted to an error in the volumetric flow rates of $\Delta \dot{V} / \dot{V} = \pm 0,02$. This is also reflected in the uncertainty bounds of the calibration factors B_1 and B_2 given in the text above.

The evaluation of the signals of the bent probe at position z = 0.275 m (see figure 3) needs a different procedure for mainly two reasons. 1) The probe lacks a second pair of thermocouple wires to compensate in case of dynamo action the signal of the main pair near the permanent magnet at the probe tip. 2) The probe tip is located near the outer channel wall in a rather non-uniform outlet flow of a bent, for which no general correlation to the volumetric flux density is available. Therefore no conclusion on the absolute value of the local mean velocity can be drawn.

We approached the first issue by measuring the mean local magnetic induction and its spatial orientation in the vicinity of the PM-probe 2. For this we moved the traversable Hall sensors along the module axis to the position *z = 0.275 m*. In this arrangement there was a distance of *l = 0.19 m* between the tip of the PM-probe and the Hall sensors. We assumed that the measured intensity and orientation of the local mean magnetic induction at the position of the Hall probes did not change in a first approximation and holds also for the position of the PM-probe 2. Furthermore, with the

help of a Hall sensor we measured the intensity and orientation of the magnetic induction of the permanent magnet along the circumference of the probe tip after the instrumentation had been removed from the test module. Thus knowing, in a reasonable approximation the intensity and orientation of the dynamo magnetic field at the tip of the PM-probe 2 and the intensity and orientation of the sensor magnet, we suggest the following relationship between the signal of the PM-probe 2 and the local mean velocity (employing Ohm's law in moving conductors)

$$\overline{u}_{C2} \sim \frac{\overline{E}_{C2}}{B_{PM} + B_D \cdot \sin\beta}. \qquad \text{(A3)}$$

Where B_{PM} is the maximum intensity of the permanent magnet, B_{Dyn} the measured absolute value of the dynamo induction field measured by the Hall probes at position z = 0.275 m on the module axis and β the angle between the orientations of the two magnetic fields. B_D and β generally change as the intensity of dynamo action changes.

Relationship A3 has been used in section 4.2 to assess the relative change of the local velocity at the tip of PM-probe 2 under the influence of the dynamo magnetic field.

A simple error analysis for the evaluation-relationship A3 may be based on estimated error bounds for the measured quantities B_{PM}, B_D, β, E_2. The maximum intensity of the permanent magnet was repeatedly measured to yield $B_{PM}=(400\pm20)$[Gauss].

The relative change of the intensity of the dynamo magnetic field B_D and its orientation γ between the position of the Hall probe and the PM-probe 2 may be assessed by the measured variation of both quantities on the module axis (see figure 4) for the same distance. This distance is $l=0,17m$. From our measured intensity distributions

(figure 4) we estimate conservatively the relative change and potential error for B_D in relationship A3 as $\Delta B_D/B_D \approx 0{,}35$ and the relative change in the angle of orientation as $\Delta\gamma/\gamma \approx 0{,}5$ The error of the measuring chain for the induced voltage E is estimated as $\Delta E/E \approx 0{,}03$. The overall relative error of the evaluation-relationship A3 is thus governed by the uncertainty of the intensity of the dynamo magnetic field at the location of the PM-probe and may be assessed, based on A3, roughly by just this error as $\Delta u/u \approx \pm 0{,}2$.